Classification and Characterization of Tropical Precipitation Based on High-Resolution Airborne Vertical Incidence Radar. Part II: Composite Vertical Structure of Hurricanes versus Storms over Florida and the Amazon

BART GEERTS AND YU DAWEI

University of Wyoming, Laramie, Wyoming

(Manuscript received 6 September 2003, in final form 20 May 2004)

ABSTRACT

High-resolution airborne measurements of vertical incidence radar reflectivity and Doppler velocity, as well as coincident upwelling 85-GHz radiances, are analyzed for several Atlantic hurricanes and for numerous convection-generated systems in Florida and Amazonia. Characteristic reflectivity, hydrometeor motion, and vertical air motion profiles of convective and stratiform precipitation are compared and related to their ice-scattering signature, with an emphasis on the difference between hurricanes and convection-generated storms. Hurricanes are found to be largely and clearly stratiform, displaying a remarkably narrow echo and vertical velocity spectrum. Air currents are inferred to be rising steadily at all levels, even in stratiform regions. Land-based, convection-generated stratiform regions tend to experience low-level descent and mid- to upper-level ascent, although the vertical velocity variability is large. Florida storms produce little stratiform precipitation. Their spectrum of echo and updraft strengths is broad, including some of the highest reflectivities aloft, resulting in very low 85-GHz radiances. Amazonian storms are relatively weak and are more ''maritime'' in echo, vertical velocity, and ice-scattering characteristics, compared to those in Florida, especially during a westerly low-level wind regime.

1. Introduction

In the first part of this study (Geerts and Dawei 2004, hereafter Part I), high-resolution vertical incidence airborne radar reflectivity data were used to classify precipitation types and assess the classification. Three rain types were distinguished—stratiform, convective, and shallow—based on the melting-layer signature that unequivocally identifies stratiform precipitation. We now use this classification to document the vertical structure of precipitation in several hurricanes. We also describe convective systems sampled in central Florida and in the southwestern corner of the Amazon basin. The composite vertical structure of these land-based systems is contrasted against that in the hurricanes.

The data on which this study of tropical precipitation systems is based (some 21 231 km of high-altitude aircraft data from three different field campaigns) do not constitute a climatology, but the dataset allows, with some degree of generality, a characterization of rain types at a resolution and sensitivity considerably better than that of wind profilers or that of the Precipitation Radar (PR) aboard the Tropical Rainfall Measuring Mission (TRMM) satellite. As such, this survey complements work based on data from TRMM, which since December 1997 has been building a global low-latitude climatology of vertical incidence radar reflectivity and coincident passive microwave data (Kummerow et al. 2000).

The high-altitude aircraft data mainly consist of nadir beam reflectivity and radial velocity from the Earth Resources (ER) Doppler radar (EDOP), as described in Part I. We also use data from a microwave radiometer aboard the same aircraft. The 85-GHz brightness temperature (T_b) has been used extensively to describe tropical precipitation systems (e.g., Mohr et al. 1999; Cecil et al. 2002). This is because it is a measure of the intensity of deep precipitation systems, which relates to the fact that ice crystals scatter the radiation upwelling from underlying droplets and from the earth's surface (Mohr and Zipser 1996).

From a climatological perspective, the drawback of the radar/passive microwave dataset is that it only covers a small number of storms and a small window of the diurnal cycle (between 1200 and 1800 LST), and that the flights preferentially tracked over the larger, longer-lived precipitation systems. Over land there was some bias toward the more intense systems, although the most intense echoes were avoided and many smaller, shallower storms were sampled fortuitously. The dataset used herein, therefore, cannot be used to describe the diurnal cycle of tropical precipitation (e.g., Nesbitt et al. 2003) or to describe the relative frequency of systems ?1

Corresponding author address: Dr. Bart Geerts, Department of Atmospheric Sciences, University of Wyoming, Laramie, WY 82071.
E-mail: geerts@uwyo.edu

by size or intensity (e.g., Rickenbach and Rutledge 1998).

Mature hurricanes are characterized by an inner-core eyewall, in which convective precipitation dominates, and a broader, mostly stratiform region outside the sloping eyewall (Jorgensen 1984; Marks 1985; Marks and Houze 1987; Houze et al. 1992; Bister and Emanuel 1997). That stratiform region is far from uniform, it tends to contain arc-shaped rainbands (Marks 1985), which may contain convective cores. Further out from the eye, at radii over about 100 km, spiral bands may occur, including a band connecting the inner eyewall to the outer principal band (Willoughby et al. 1984). These bands tend to be more stratiform toward the core and more convective outward.

Precipitation characteristics of nonhurricane tropical precipitation systems have been studied extensively, both over land and ocean, thanks to a series of focused field campaigns (e.g., Cheng and Houze 1979; Churchill and Houze 1984; Leary 1984; Chong and Hauser 1989; Goldenberg et al. 1990; Steiner et al. 1995; Short et al. 1997; Rickenbach and Rutledge 1998; Yuter and Houze 1998; Rickenbach et al. 2002). Different levels of organization have been documented, and most systems, except isolated convective cells, develop some stratiform precipitation, either adjacent to active cells or as the storm decays. Young, vigorous convective regions usually evolve into regions of decaying convection, in which the vertical air motions are smaller and reflectivity profiles develop a bright band (BB; Houze 1997). A global view of the Tropics suggests that stratiform regions are more common over the oceans, while over land relatively larger convective rain amounts and higher convective rain rates occur (Schumacher and Houze 2003a).

The data source is described next. Regional differences in the composite vertical structure of precipitation systems are discussed in section 3, and these are interpreted in the context of other, mostly TRMM-based observations in section 4.

2. Data sources

This study is based on all data from three field campaigns in which the National Aeronautics and Space Administration (NASA) ER-2 targeted tropical precipitation systems. The flight tracks selected are those that are level and that had two instruments in operation: ?2 EDOP (Heymsfield et al. 1996) and the Advanced Microwave Precipitation Radiometer (AMPR). One campaign focused on tropical depressions and cyclones in the Atlantic and the Gulf of Mexico (14 437 km of flight tracks, referred to as the ''hurricane'' sample), one sampled summertime thunderstorms over central Florida (2183 km of flight tracks, referred to as ''Florida''), and one examined precipitation systems over Rondonia in the southwestern corner of Brazil, in the austral summer (4611 km of flight tracks, referred to as ''Brazil'').

The key dataset is the EDOP nadir beam reflectivity and radial velocity profiles. The processing of the radial velocities is described in Part I, including the correction for aircraft motion and for a bias due to the antenna's orientation slightly off nadir. Part I also describes how hydrometeor fall speed and vertical air motion are estimated, and how the reflectivity profiles are used to classify precipitation into warm (shallow) rain and deep convective or stratiform precipitation.

In addition to EDOP, the ER-2 carried the four-channel AMPR (Spencer et al. 1994). The four frequencies (10.7, 19.4, 37.1, and 85.5 GHz) have a sea level field of view (FOV) of 2.8, 2.8, 1.5, and 0.6 km, respectively, for a flight level of 20 km. Mainly, the 85-GHz channel is used in this study. The reasons are that this channel is less affected by earth surface emissivity variations than other channels, and that it best matches the EDOP footprint. The 85.5-GHz-radiometer FOV is slightly smaller than the EDOP FOV, which is 0.8 km at 5 km; however, the sensitivity to features within the FOV differs: the two-way (radar) beam illumination function drops off faster from the beam center than the one-way (passive microwave) function. The result is that the FOV of the EDOP profiles corresponds best with the FOV of the 85.5-GHz channel. Also, and most importantly, the 85.5-GHz T_b has been used extensively as a measure of the intensity of tropical precipitation systems.

AMPR is a cross-track scanning instrument, but only the nadir data are used. The AMPR sampling frequency at nadir is 2–3 s, which implies a displacement of 400–600 m along the flight track. In this study, EDOP and AMPR data are merged. In the merged data files a single nadir AMPR observation is repeated approximately 5 times for each EDOP profile. Even though a time difference of up to 2 s may exist between merged AMPR and EDOP data, the FOV for each matched pair compares reasonably well because of EDOP's oversampling; EDOP profiles are collected every 0.5 s or 100 m, a distance that is smaller than the beam diameter (800 m at a height of 5 km). The surface footprints of two nadir EDOP beams separated by 3 s still have a nearly 50% overlap. Also, the ER-2 is a stable platform, and high-frequency ($<$3 s) variations of roll or pitch are generally less than 0.2°. In other words, the part of the variability in any relationship between an EDOP-derived variable and an AMPR-derived variable that is due to natural finescale variations sampled by one instrument and not by the other should be small.

3. Characteristic radar profiles and passive microwave signatures in tropical precipitation

Tropical precipitation, classified according to rain type (Part I), is now characterized in terms of composite profiles of reflectivity and vertical velocity, and in terms of the relationship between the 85-GHz T_b and storm intensity parameters. The purpose is not only to contrast stratiform versus convective and shallow rain profiles,

but also to highlight the differences between ordinary convective storms and hurricanes. The stratiform samples analyzed here only include the stratiform-certain profiles (see Table 2 in Part I), in order to focus on the contrast with convective profiles.

EDOP profiles will be summarized by means of frequency-by-altitude diagrams (FAD) of nadir-beam reflectivity, radial velocity, and derived vertical air motion. These FADs are probability density functions, that is, they show the ''normalized'' probability of encountering a given value bin at a given height. It is normalized in the sense that the integral of all probabilities, over all values and all levels, equals 100. This is different from the contoured FADs (CFADs) in Yuter and Houze (1995), which normalize the distributions by the number of occurrences at each level. The drawback of such a display is that it only shows the relative frequency of a value at any given height; it does not reveal the variation of occurrences with height.

For deep precipitating systems, the maximum reflectivity, the echo-top height, and the reflectivity at some level above the freezing level are all indicators of scattering of the upwelling 85-GHz radiance by ice particles, which suppresses the 85-GHz T_b. Toracinta et al. (2002) and Cecil and Zipser (2002) use the echo-top and 7-km reflectivity to describe precipitation system characteristics in the global Tropics, by means of TRMM PR and TRMM Microwave Imager (TMI) data. Toracinta et al. (2002, their Fig. 4) show that the 85-GHz T_b tends to be lower for higher 7-km reflectivity over tropical oceans and in tropical South America. Cecil and Zipser (2002, their Fig. 7) demonstrate a negative correlation between the 85-GHz T_b and the maximum height of the 30-dBZ contour (a measure of echo-top height) both in continental and oceanic tropical systems. We will explore these relationships, but at a higher resolution and stratified by rain type.

Characterizations of convective and stratiform precipitation are now presented for the EDOP–AMPR dataset. Dynamically, a mature hurricane is a balanced vortex close to neutral symmetric stability, sustained by surface fluxes. The storms sampled in Brazil and Florida are short-lived, buoyancy-driven systems, with limited mesoscale organization.

a. Tropical cyclones and depressions

Several Hurricanes (Bonnie, Earl, Georges) and one tropical depression were sampled in the third field campaign of the Convection and Moisture Experiment (CAMEX-3). The ER-2 flew straight tracks across the center of the circulation at various azimuths to a maximum radius of 100–150 km, depending on the size of the storm (e.g., Geerts et al. 2000).

A transect across Hurricane Bonnie is shown in Fig. 1, as an example. A BB is clearly visible, above which the reflectivity decreases sharply. Another melting-layer signature is the large radial velocity gradient coincident with the BB. In some regions the cloud top is close to the BB. The right (northern) eyewall at $160 < x < 220$ km is much weaker than the left (southern) one, which contains some convective regions. The upper-level updraft cores in the left eyewall (0–30 km in Fig. 1) suggest some regions of buoyant ascent in the ice region. Shallow or ''warm'' rain occurs on the northern side of the eyewall, below an anvil. The AMPR 10-GHz emissivity over oceans is low, and more elevated 10-GHz T_b values indicate emission from cloud and/or raindrops (Kummerow et al. 1991). Indeed the three 10-GHz T_b spikes between 70 and 120 km in Fig. 1 correspond to reflectivity maxima below the freezing level. The 85-GHz T_b is reduced by ice scattering, for instance, between 0 and 30 km in Fig. 1. The magnitude of this deficit corresponds well to vertically integrated reflectivity above the BB (Cecil and Zipser 2002). In this transect the 85-GHz T_b reaches a low of 200 K, which is high compared to most continental mesoscale convective systems (MCSs; Mohr and Zipser 1996).

The prevalence of stratiform precipitation in this transect applies generally: some two-thirds of the EDOP profiles in the hurricane sample are stratiform, while only 19% is convective (Table 2 in Part I). It is noteworthy that when EDOP profiles are downgraded to a resolution of 125 m, the hurricane sample loses less than 1% of the BB profiles, compared to about 5% for the ordinary convective systems in Florida and Brazil (Fig. 4 in Part I). It was found also that the two melting-layer signatures that define stratiform precipitation, that is, the presence of a BB and a large radial velocity gradient, agree best for the hurricane sample (Table 3 in Part I), and that only for Hurricane stratiform profiles does reflectivity continue to clearly decrease with height above some 300 m above the BB (Fig. 6 in Part I). These are all indications of the unambiguously stratiform nature of the hurricane stratiform profiles.

The stratiform precipitation is quite uniform in the Hurricane sample; its FADs of the reflectivity, the radial velocity, and vertical air motion are narrowly distributed (Fig. 2). This is consistent with the long-lived nature of hurricanes. Reflectivity decays rapidly (4–5 dB km^{-1}) above a well-defined BB. Individual stratiform profiles too feature this nearly constant decay rate up to the echo top. As a result, profiles with a brighter BB have a proportionally higher 7-km reflectivity and a higher echo top.

The mean reflectivity of the stratiform profiles increases slightly with depth below the freezing level (Fig. 3), suggesting that raindrops continue to grow as they fall, either by coalescence or condensation. The true BB is thinner than suggested in the FAD, because of variations of the freezing level across a tropical cyclone. Also, the height shown in Fig. 2 and others is relative to the echo maximum signifying the earth's surface, which is the sea level in all cases (except for some transects across the mountainous island of Hispaniola on 22 September 1998; Geerts et al. 2000). In other

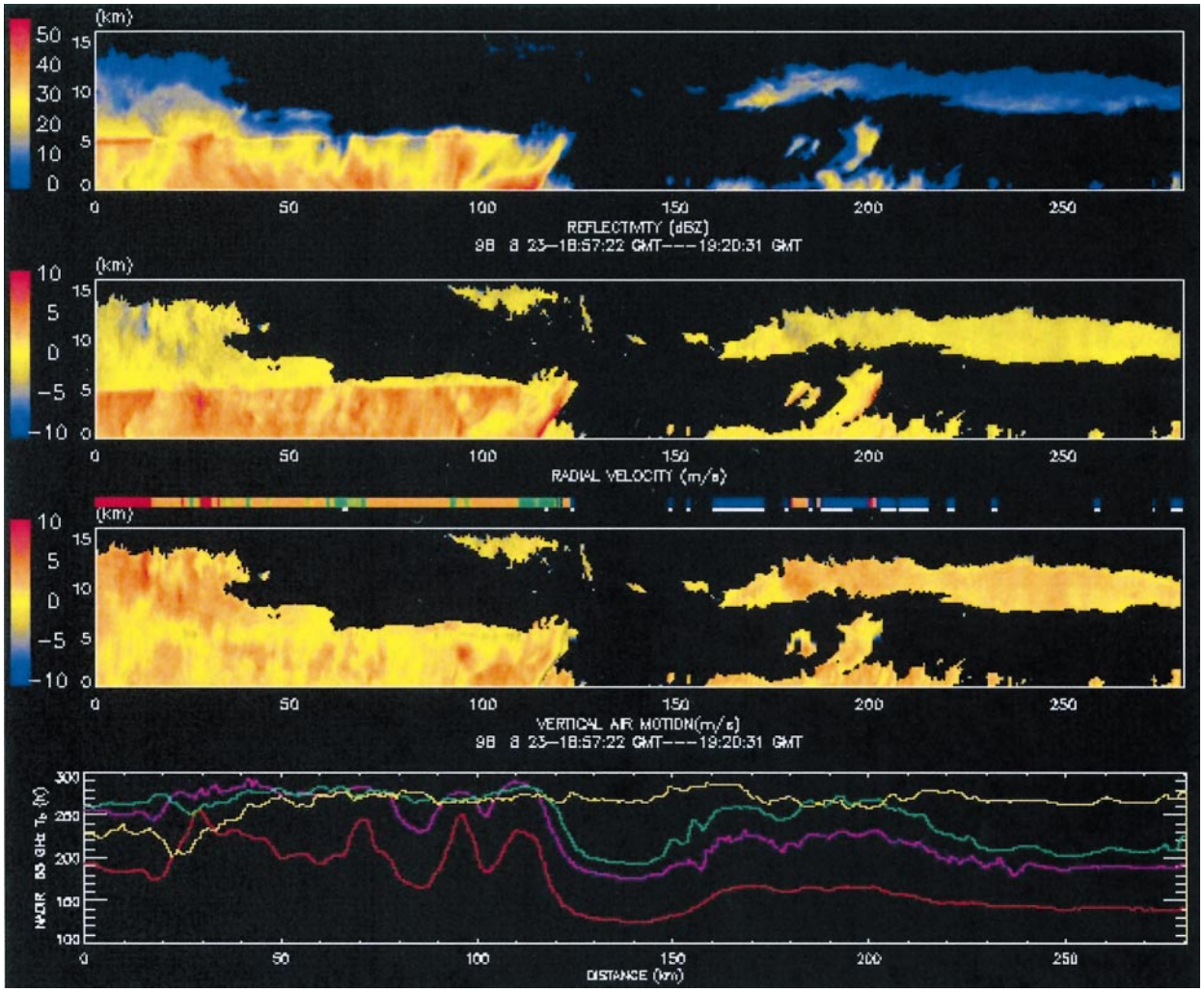

FIG. 1. A cross section of the eyewall and eye of Hurricane Bonnie at 1857–1920 UTC 23 Aug 1998. The eye is centered at a distance of 140 km on the *x* axis. The vertical axis for the first three images is height above sea level (km), as detected by EDOP. From top to bottom, the images display: (a) EDOP nadir reflectivity (dBZ), (b) the radar radial velocity corrected for aircraft motion (this is the hydrometeor vertical velocity, m s^{-1}, downward is positive), (c) air vertical velocity (m s^{-1}), and (d) coincident AMPR microwave brightness temperatures at 10, 19, 37, and 85 GHz. The latter are shown by lines in red, purple, green, and yellow, respectively. On the rain-type classification bar shown between (b) and (c): stratiform-certain rain (red), stratiform-probable rain (orange), convective rain (green), inconclusive rain (blue), and virga (purple; see Fig. 2 in Part I for definitions). Black means no rain. The white line under this bar indicates locations of warm rain, which can be convective or inconclusive.

words, even more uniformity is evident if the height is plotted relative to the BB (Fig. 6 in Part I).

In convective profiles, the rate of decay of reflectivity above the freezing level is, on average, only slightly smaller (Fig. 3), yet it is more variable than for stratiform profiles (Fig. 2). The latter is consistent with the higher variability of radial velocity. Convective echo tops are generally at the same height as stratiform ones, only on a few occasions they are higher. At low levels, many convective profiles have a lower reflectivity than typical stratiform values. The average reflectivity of hurricane convection between 1- and 4-km altitude is only 32.2 dBZ, which is merely 1.5 dBZ higher than that of stratiform profiles (Fig. 3). This contrasts with MCSs, in which the convective/stratiform distinction typically is much larger. The hurricane convective reflectivity FAD shows a clear change in slope at the freezing level (Fig. 2), and its radial velocity gradient around the freezing level is rather large (Fig. 3). This suggests that the hurricane convective profiles are close to the melting-layer signature of stratiform precipitation.

The reflectivity FAD also shows that convective echoes become more frequent toward the ground below the freezing level, unlike the stratiform echoes. This is due to warm rain. The 8% of the hurricane profiles that is classified as warm rain (Table 1) not only occur in the eye, but also on the suppressed side of asymmetric eyewalls (Fig. 1). This implies that while deep ascent pre-

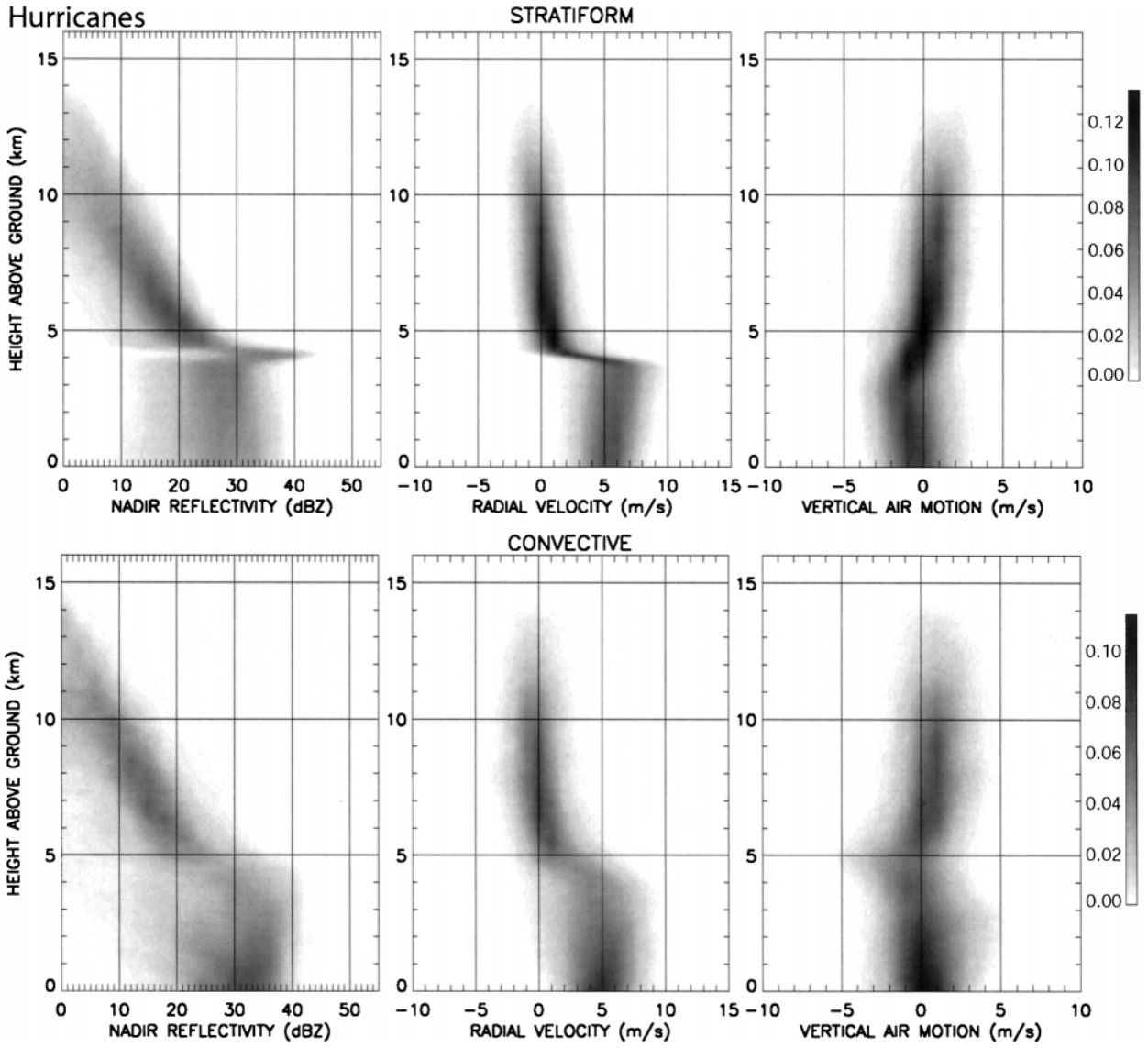

FIG. 2. Frequency-by-altitude display of the nadir reflectivity, radial velocity, and vertical air motion (m s^{-1}) for (top) stratiform and (bottom) convective rain, based on all hurricane surface rain profiles. The height is the altitude above sea level. The units of the frequencies shown are (left panels) (3 dBZ)$^{-1}$ km^{-1} and (center and right panels) (m s^{-1})$^{-1}$ km^{-1}.

vails, some regions in hurricanes experience only shallow ascent.

Most of the snow in the hurricanes sample rises at some level, both in convective and in stratiform profiles, and lofting over a depth of at least 3 km occurs in 11% of the profiles. The mean hydrometeor vertical motion (i.e., the negative of the radial velocity in Fig. 2) increases from -1.2 to $+1.0$ m s^{-1} between 5 and 11 km for convective and stratiform profiles, which differ little (Fig. 3). While these values are close to the radial velocity uncertainty (section 2c in Part I) in an absolute sense, the vertical trend is accurate. Because the fall speed of snow at 5 km is close to 1.2 m s^{-1}, updrafts must prevail above the freezing level in hurricanes. This is apparent in the FADs of vertical air motion (Fig. 2, rightmost plots). Ascent tends to occur at low levels as well, increasing to 2.6 m s^{-1} on average at 11 km. In short, widespread uplift is found at all levels in hurricanes, and the rate of ascent differs little between stratiform and convective profiles (Fig. 3). The vertical air motion in convective profiles is more variable, but again ascent occurs at all levels, peaking at an average value of 2.9 m s^{-1} between 9- and 12-km altitude.

The 85-GHz T_b over hurricanes is generally high compared to midlatitude MCSs (Mohr and Zipser 1996), consistent with the rapid decay of reflectivity with height above the BB. As expected, it tends to decrease with increasing echo-top height and increasing 7-km reflectivity Fig. 4). This relationship is slightly stronger for hurricane convection than for stratiform profiles. The

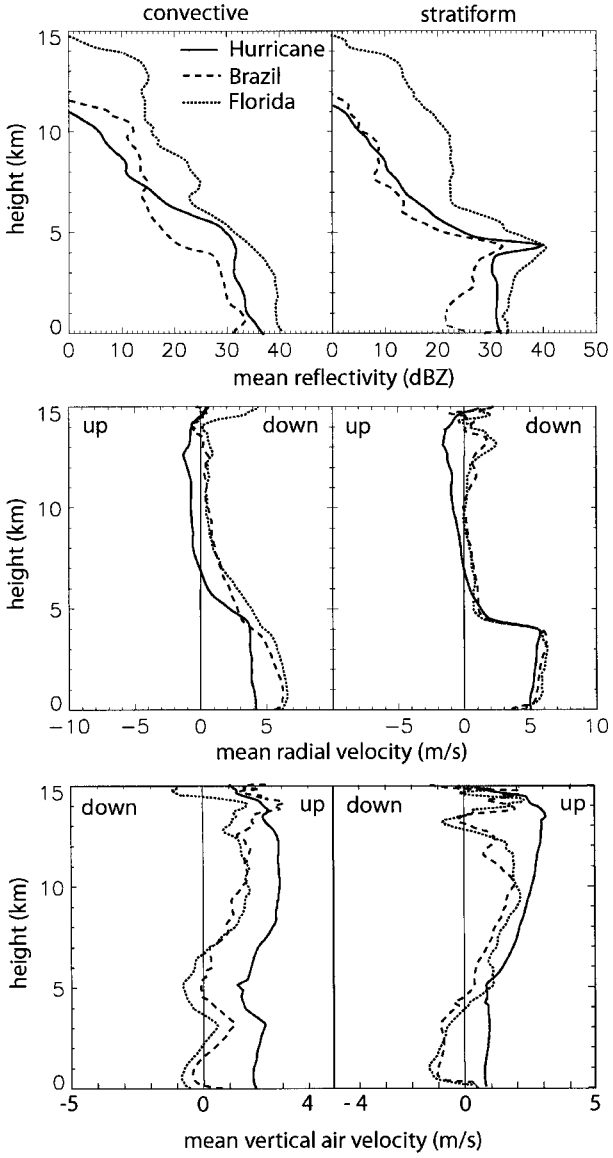

FIG. 3. Mean profiles for all (left) convective and (right) stratiform certain in the three campaigns. The sample size decreases with height mainly between 10 and 15 km; therefore, the upper-level values are less representative.

85-GHz T_b also tends to be lower when the maximum reflectivity is higher (Fig. 4), but especially in stratiform profiles this relationship is weak, possibly because of abundant supercooled water.

Surprisingly, the relationship between 85-GHz T_b and 7-km reflectivity is not linear, for both convective and stratiform regions. The 85-GHz T_b deficit seems unaffected by 7-km reflectivity if the latter remains under 10–15 dB*Z*. It is not clear why this is the case, but at least this is below the 18-dB*Z* sensitivity threshold of the TRMM PR. But, even at higher 7-km reflectivity values, the scatter is generally broad, even though the hurricane sample is quite uniform in terms of reflectivity

TABLE 1. (a) The number of profiles with precipitation not reaching the ground (virga), and (b) the number of warm rain profiles, for three regions. The numbers are also expressed as a percentage of all rain profiles listed in Part 1, Table 1 for each region. The fraction of warm rain profiles that is classified as convective is shown as well, the remaining profiles are inconclusive.

	No. of profiles		
	Florida	Hurricane	Brazil
a. Virga			
Tot	7461	13 809	4976
Virga fraction	49%	11%	20%
b. Warm rain			
Tot	593	10 049	2072
Warm rain fraction	4%	8%	8%
Convective warm rain	46%	58%	44%

and velocity profiles. The rather poor relationship between reflectivity-based storm intensity and 85-GHz T_b, as revealed by high-resolution data, suggests that the 85-GHz T_b is quite sensitive to cloud microphysical aspects that are not captured by radar reflectivity, such as the crystal habit or amount of supercooled water.

b. Convection-generated cumulonimbus

Cumulonimbus cells or clusters of cells were sampled in various stages of their life cycle in central Florida and the southwestern Amazon.

1) CENTRAL FLORIDA

Summertime convection in central Florida generally breaks out along shallow boundaries and is short lived (e.g., Kingsmill 1995). The convection is quite intense and strongly modulated by daytime heating over land. Low-level ambient wind shear is generally weak; hence, long-lived mesoscale organization is quite rare. Many storms in the Florida dataset were overflown in their mature to dissipating stages, but some vigorously developing storms were captured as well. In one case the ER-2 traversed a sequence of storm cells triggered by the convergence of two shallow boundaries (Fig. 5). The point of boundary collapse (the ''zipper'') moved from north to south, and a north–south flight leg documented a series of age-ordered cells, with the youngest one to the south (right). Between the collapsing and vigorously growing convection, a small region of upper-level mesoscale upward motion can be seen; however, this region does not produce stratiform precipitation at this time.

Tropical disturbances, bringing more stratiform widespread precipitation, may also occur over central Florida in summer, but the 2183 km of flight tracks that constitute the Florida dataset only include small, short-lived, surface-triggered afternoon thunderstorms, except for one more long-lived, larger, mostly stratiform system with embedded convection (on 5 September 1998).

Convective precipitation dominates over central Flor-

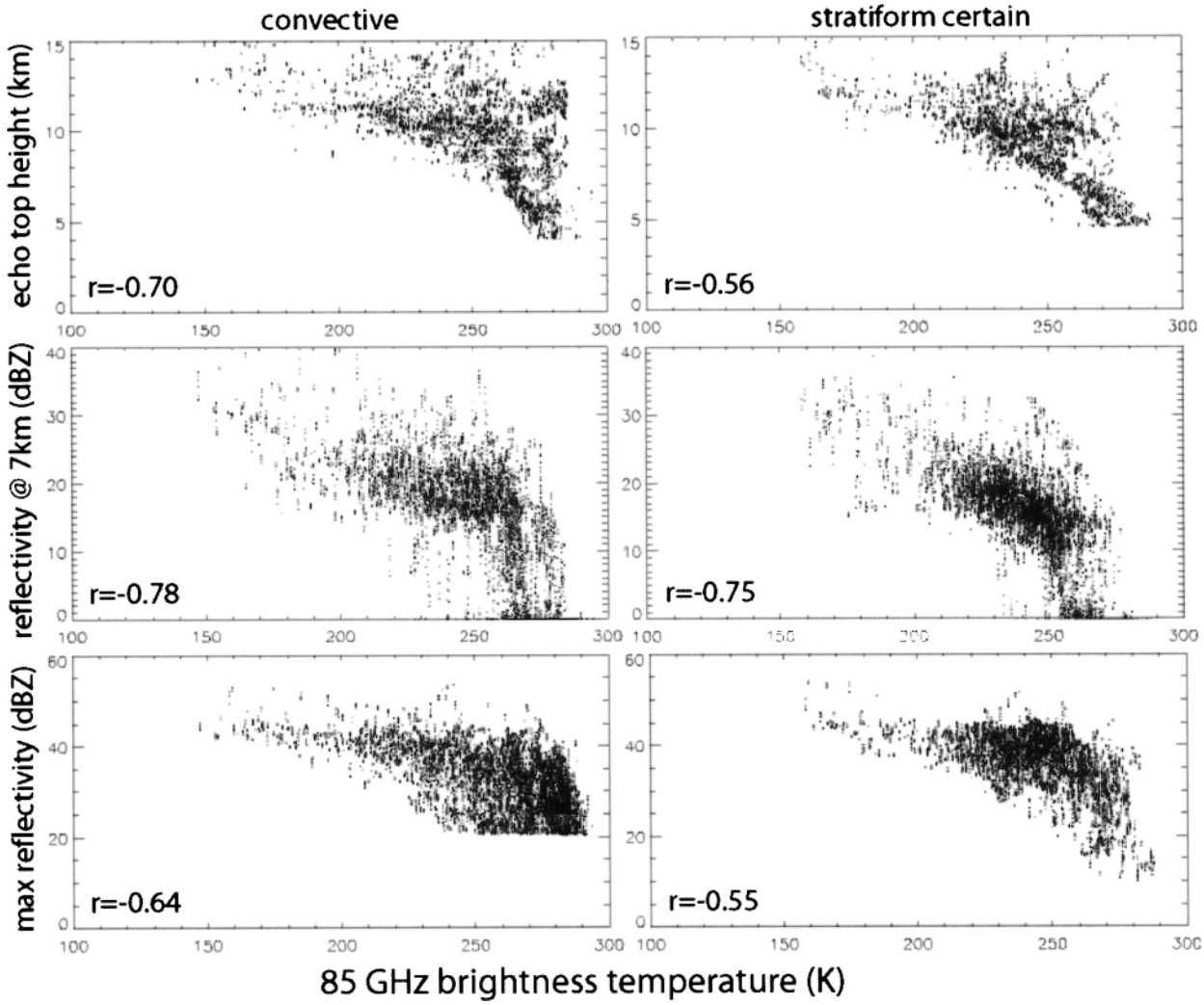

FIG. 4. Scatterplots of the 0-dB*Z* echo-top height (km), reflectivity at a height of 7 km, and maximum reflectivity in the profile, against 85-GHz brightness temperature, for all (left) convective and (right) stratiform surface rain profiles in the hurricane sample. The linear correlation coefficient *r* is listed in each plot.

ida (Table 2 in Part I), but about half of all rain profiles contains only virga (Table 1). This suggests that convective cells have a lifetime that is short compared to that of the anvils that they generate, and this in turn is probably related to the intensity of Florida thunderstorms—more vigorous storms can inject more ice into the upper troposphere. A sample transect (Fig. 6) shows two vigorous storm cells. (This transect does not show any large anvil or BB regions.) The left storm cell tops at an altitude of 14.8 km and has a minimum 85-GHz T_b of 117 K, consistent with a deep layer of frozen hydrometeors. This cell, about 15 km wide, has no less than six updrafts peaking at over 5 m s^{-1}, interspersed between downdrafts. The strongest updraft continues into the overshooting top seen in the reflectivity field. Clearly, the hydrometeor vertical motion is quite variable, and several elevated reflectivity maxima exist. The fine structure and the lack of vertical continuity of these updrafts are remarkable. Clearly the retrieval of vertical air motion from scanning ground-based dual-Doppler data cannot be easy, whichever boundary condition is used (Chong and Testud 1983).

We now examine the composite of Florida precipitation systems sampled during the Texas and Florida Underflights (TEFLUN-B) field experiment. This sample size is the smallest, so some caution is warranted regarding statistical significance. The contrast between Florida cumulonimbus and the hurricane sample is stark; the stratiform area fraction (along the ER-2 flight tracks) is much smaller, more profiles are classified ''stratiform probable'' than ''stratiform certain'' (Table 2 in Part I), and the stratiform profiles display more variability (Fig. 7). This profile suggests that most of these stratiform regions are the remnants of decaying storm cells, for two reasons. First, the reflectivity profile is highly variable, suggesting that the EDOP sample covers a range

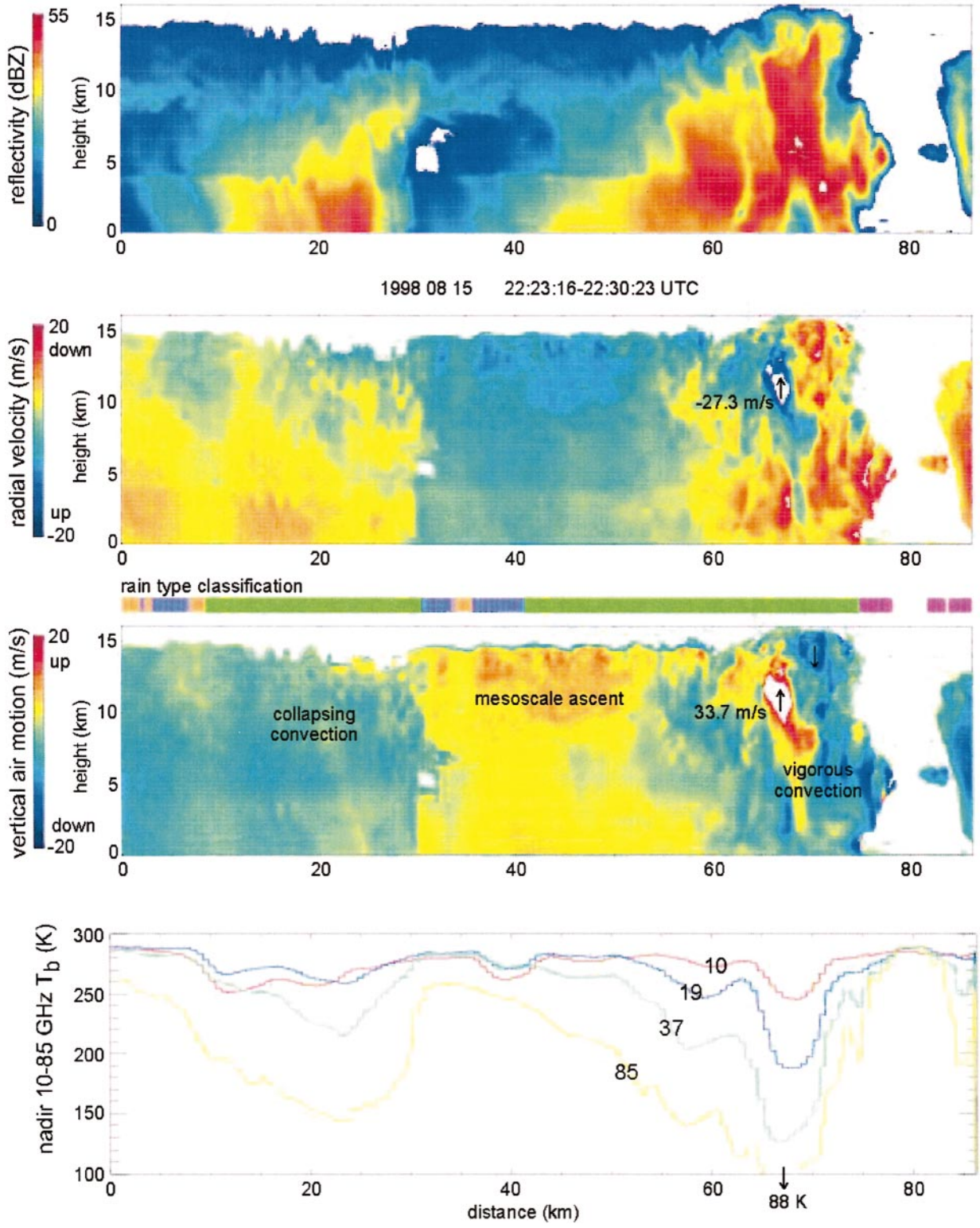

FIG. 5. As Fig. 1, but for 15 Aug 1998 in central Florida. The transect is from (left) north to (right) south.

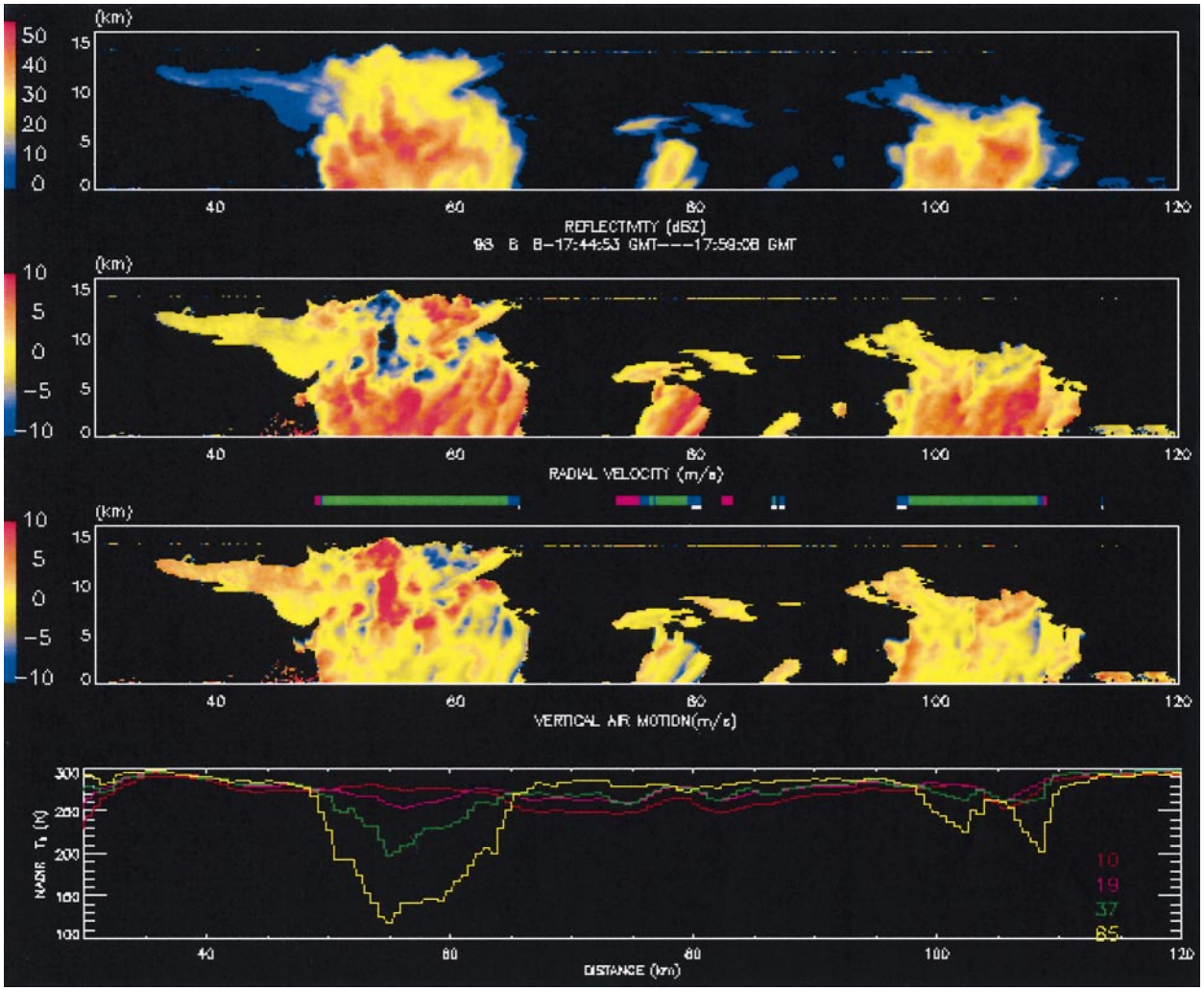

FIG. 6. As Fig. 1, but showing deep convection in central Florida at 1744–1755 UTC 8 Aug 1998. The intermittent line at ~14 km is the range-folded triple-reflected echo of the ER-2 aircraft.

of phases in the convective-to-stratiform transition. And second, the reflectivity decay with height above the BB is small—the mean reflectivity of the stratiform Florida profiles decays at ~2.7 dB km^{-1} between 5- and 13-km altitude (Fig. 3). Such decay of reflectivity, which matches that observed in a stratiform region of an MCS in Kansas (Houze 1997, his Fig. 11c) is less even than that for the convective hurricane profiles (Fig. 2). This suggests that large particles have been carried aloft; in other words, the profile may reflect a history of stronger updrafts. Such updrafts are associated either with local decaying convection or with neighboring active convection (Houze 1997, his Fig. 1). In fact, the upper-level ascent in these stratiform regions peaks at 2 m s^{-1} or more in some 40% of the profiles (Fig. 7, upper-right panel; Table 4 in Part I). The reflectivity below the BB generally decreases toward the ground (Fig. 3), consistent with the prevailing low-level subsidence (Fig. 7, upper right), and the frequent occurrence of virga (Table 1).

A majority of Florida stratiform profiles is associated with sinking air below the freezing level, on average −1.0 m s^{-1} between 1 and 2 km, and rising air above the freezing level, on average 1.5 m s^{-1} between 9 and 11 km (Fig. 7). Such profile of vertical air velocity, characteristic of the stratiform region trailing behind long-lived squall lines (Houze 1993, p. 373), is encountered also in the Brazil sample. This suggests that the vertical velocity profile, which sustains well-organized stratiform regions of MCSs, may also be present in convectively generated stratiform precipitation with smaller space and time scales. Clearly this vertical velocity profile is not sufficiently long lived to produce large stratiform regions; the decay of convection is rather rapid, and in the end only anvils remain whose hydrometeors do not reach the ground (Table 1).

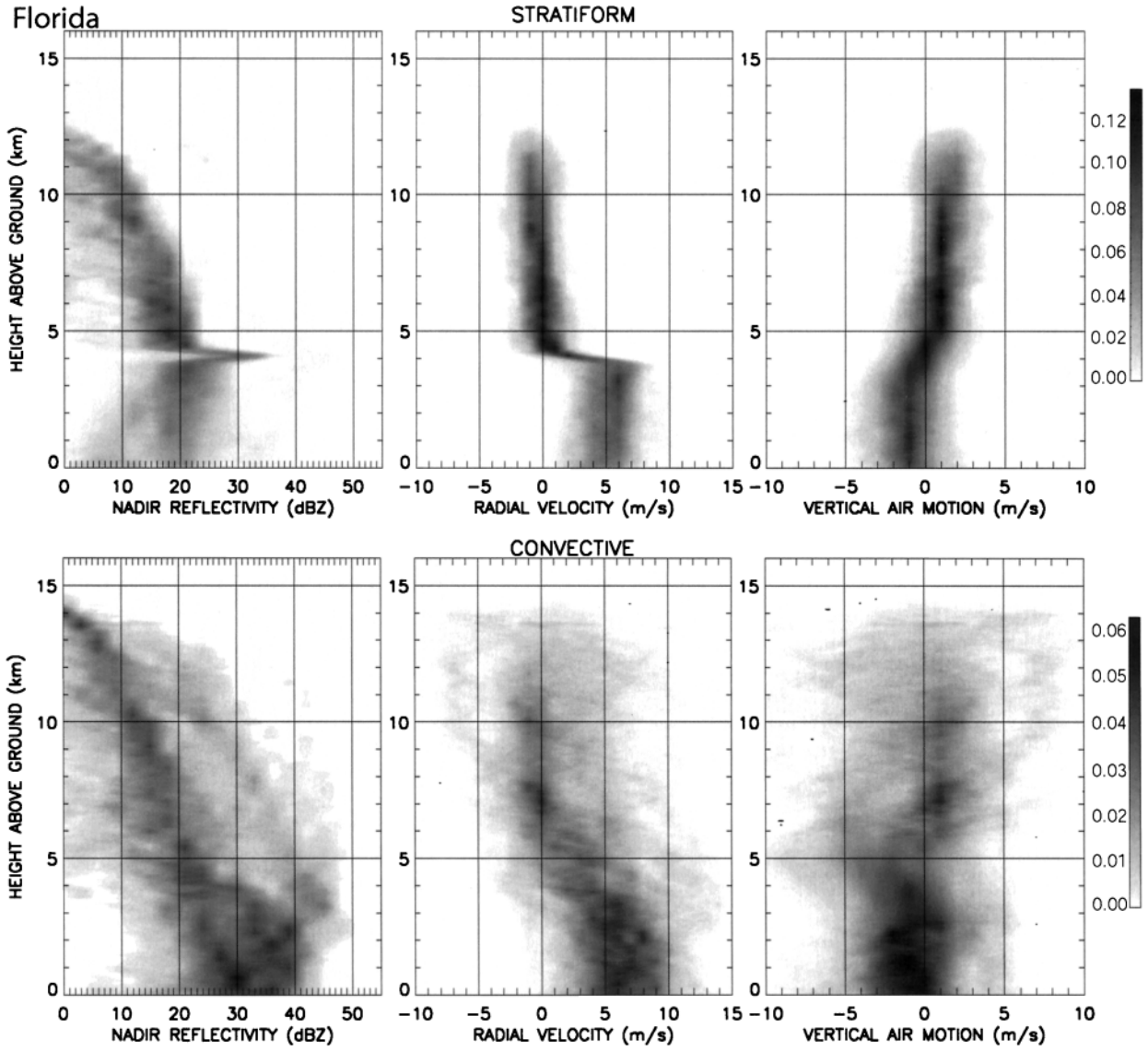

FIG. 7. As Fig. 2, but for all surface rain profiles over central Florida.

The convective–stratiform separation is quite evident in central Florida. Thunderstorms were sampled over a remarkable range of intensities and life cycle stages, as is evident in the convective FADs for reflectivity and radial velocity (Fig. 7). A clear difference between the two rain types lies in the spread of vertical motions (Table 4 in Part I) around the mean. This is consistent with the dynamical interpretation that convective precipitation is buoyancy driven.

Convective regions in Florida are unambiguously convective, for two reasons. Reflectivity distribution is quite broad in the convective region in Florida (Fig. 7). This is consistent with the large range in vertical motions there. Second, the average reflectivity in Florida convection decreases steadily with height from the ground to echo top (Fig. 3), without kink at the melting layer.

The convective reflectivity FAD is bimodal near and above the freezing level (Fig. 7). Such distribution was observed also in deep convection that developed as Hurricane Georges was centered over Hispaniola (Geerts et al. 2000), and the bimodality was interpreted as a combination of active convective cores (high reflectivity and strong updrafts) and ambient convective residue (lower reflectivity and weaker vertical drafts). The EDOP Florida dataset confirms this interpretation; at altitudes between 4 and 12 km, reflectivity and updraft correlate positively ($r = +0.23$) for convective profiles, but negatively ($r = -0.58$) for stratiform profiles.

A large range of storm intensities and depths was

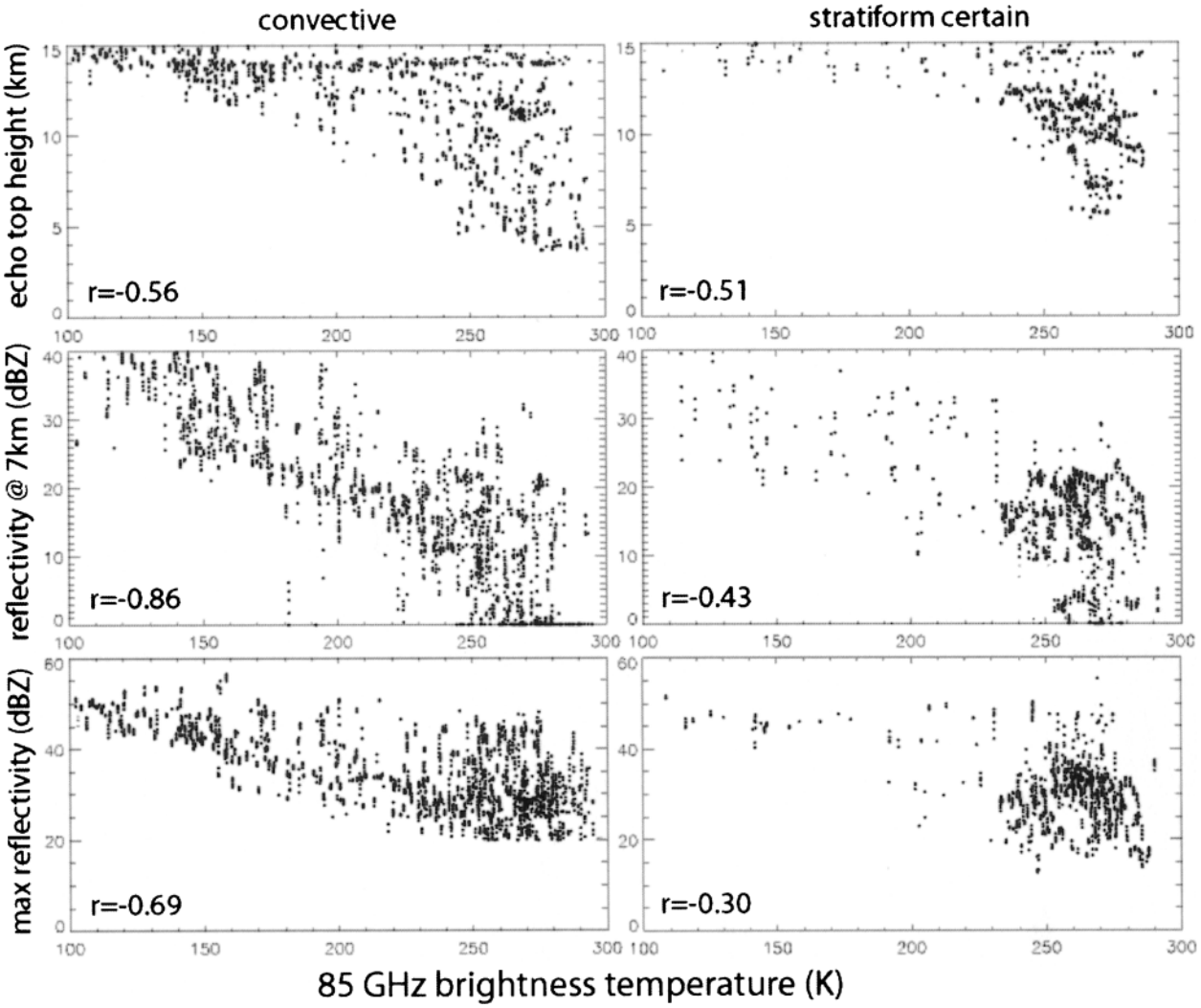

FIG. 8. As Fig. 4, but for all surface rain profiles over central Florida.

sampled in Florida, therefore, it is not surprising that the 85-GHz T_b is quite variable as well. The median 85-GHz T_b for convective profiles is 208 K, which is 21 K lower than for convective profiles in the hurricane sample. Notwithstanding the large range in 85-GHz T_b values, its correlations with storm intensity parameters are rather weak (Fig. 8). The correlations are better for convective profiles, and the 85-GHz T_b correlates best with the 7-km reflectivity, and less strongly with echo top and maximum reflectivity. Most convective regions peak near 14 km in Florida, yet any amount of 85-GHz radiation can be welling up from these regions; this is consistent with the wide range of reflectivities (and ice concentrations) below these regions. Inspection of the scatterplots in Fig. 8 reveals that the good correlations are due more to the wide range of observations, rather than to a clear alignment along a regression line. In contrast, the hurricane data are more clustered and shifted to higher 85-GHz T_b values (Fig. 4). This suggests that the convective profiles sampled in Florida have highly variable concentrations of frozen hydrometeors and supercooled water. The stratiform profiles in Florida are too few and diverse to generate reliable correlations with the 85-GHz T_b.

?10

2) PRECIPITATION IN RONDONIA, BRAZIL

A range of precipitating system sizes occurred in Rondonia, Brazil, during the TRMM component of the Brazilian Large-Scale Biosphere–Atmosphere experiment (LBA). The experimental objective was to steer the ER-2 over the larger, longer-lived precipitation systems; but, partly because the ER-2 sampled only during a narrow part of the diurnal window, none of the many large MCSs that were observed mainly in the evening by ground-based radar over Rondonia in January–February 1999 were sampled. One of the larger systems observed by the ER-2 was shown in Part I (their Fig. 3). The 85-

?11

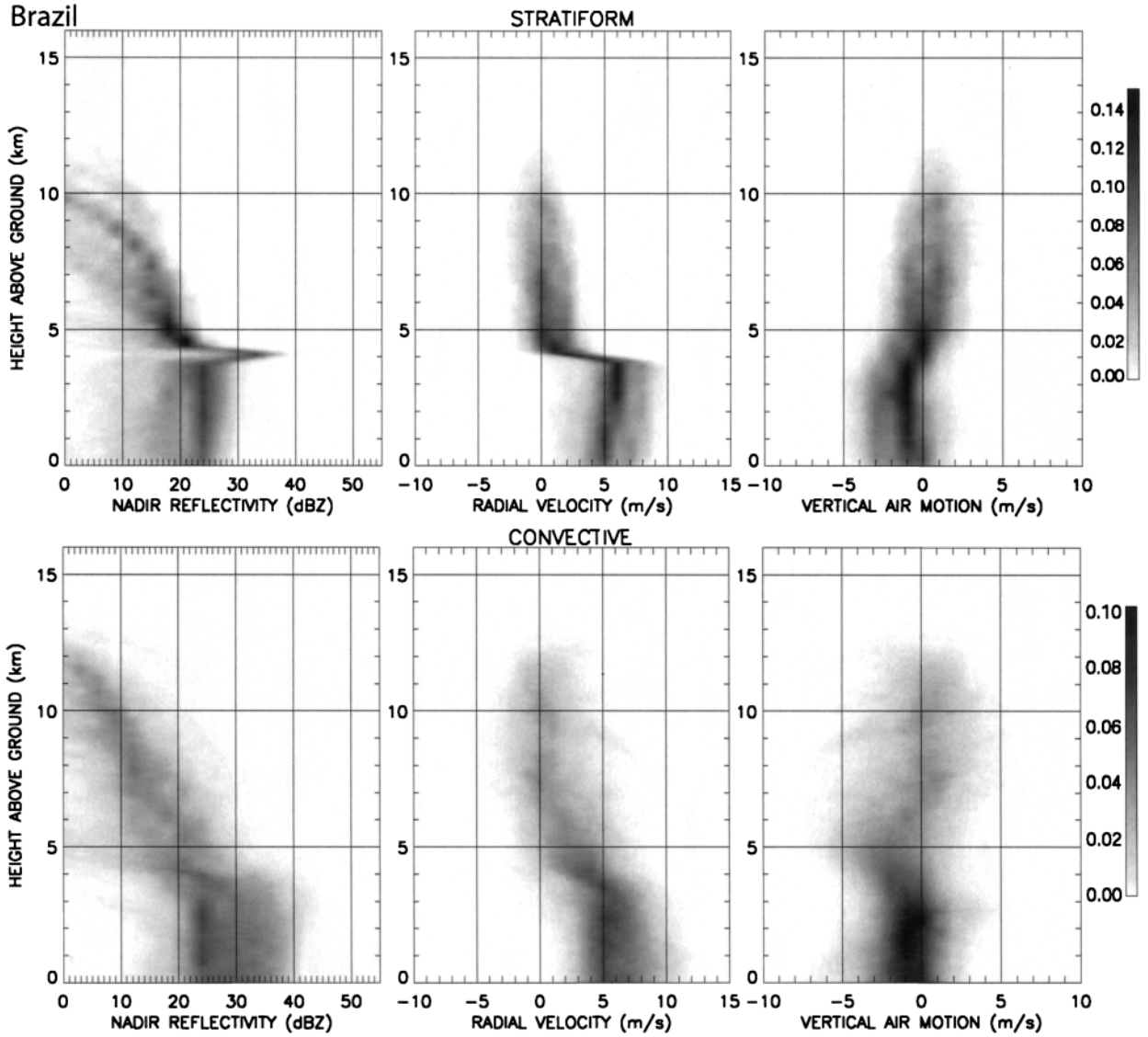

FIG. 9. As Fig. 2, but for all surface rain profiles over Rondonia, Brazil.

GHz T_b is depressed to about 190 K above the storm, but it is hardly affected by the ice in the anvil region spreading to left ($0 < x < 20$ km, Fig. 4).

Statistical characterization of Brazil precipitation is summarized in Fig. 9. The stratiform reflectivity profiles indicate high variability, comparable to the Florida (Fig. 7) profiles, but the echo tops are generally lower, and the echoes are generally weaker, especially at upper levels (Fig. 3). The reflectivity lapse rate above the BB is larger than in Florida (Fig. 7). There is a broad range of echo strengths above the BB, but a distinct population of stratiform profiles in Brazil has a rather uniform and strong echo (Fig. 9, upper left). These profiles correspond to the stratiform regions of some small MCSs. Below the BB, the reflectivity distribution is bimodal. The stronger profiles (~23 dBZ) have reflectivities below that of the BB, but clearly above that of weaker stratiform regions. The secondary maximum of weaker profiles (~18 dBZ) vanishes toward the ground. This bimodality is observed also in Florida. The explanation is not clear.

The lower reflectivity in Brazil convection (Fig. 9, lower left), compared to that in the two other regions, confirms that mostly weak systems were sampled. The variability of convective reflectivities and radial velocities, the radial velocity gradient, and the change in slope of the reflectivity profile near the melting layer all suggest that convective regions in Brazil are less robustly convective than in Florida. The rather large fraction of warm rain profiles (Table 1) may explain the increased frequency of echoes below the freezing level in convective profiles (Fig. 9, lower left). Convection in the Brazil dataset has a rather complex vertical air velocity profile, on average, with two peaks in ascent rate, one

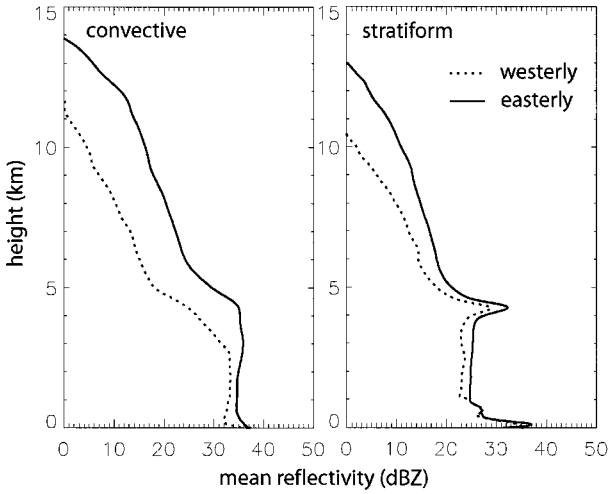

FIG. 10. Mean reflectivity profiles for (left) convective and (right) stratiform low-level flow regimes in the Brazil profile. EDOP reflectivity profiles collected on days with a westerly regime are contrasted against those during an easterly regime.

near 3-km altitude and one at upper levels. Vertical velocity variations between Florida and hurricane convection tend to follow the same trend (Fig. 3). The prevailing ascent between 1.5 and 4.5 km in the convective regions contrasts against the prevailing subsidence in that layer in stratiform regions (Fig. 3). The reason for the kink near 5 km may be questioned because the hydrometeor fall speeds are least certain at these altitudes in convection. Possibly there is more graupel at these levels then assumed (see the appendix in Part I).

Two modes of large-scale circulation occur in the southern Amazon region, yielding distinctly different precipitation systems (Petersen et al. 2002; Halverson et al. 2002). Convective intensity, lightning activity, rainfall rates, and 85-GHz T_b depression all tend to be larger during periods of low-level easterly wind, while they are lower during 850-mb westerly wind regimes. We divided the flight days in Brazil according to the day's flow regime, according to Petersen et al. (2002). Indeed, our rather small sample confirms that the mean reflectivity was higher, and storms deeper, on the days with easterly flow (Fig. 10). The difference is most pronounced for the convective profiles. The stratiform area fraction is also higher during westerly regimes (57%) than during easterly regimes (48%).

The correlations between the 85-GHz T_b and integrated ice-scattering parameters are broadly similar to those for the Florida samples (Fig. 11). The ''best'' parameter, the 7-km reflectivity, correlates better with the 85-GHz T_b in Brazil than in Florida. Again, the correlations tend to be better for convective profiles. One exception is the maximum reflectivity in convective profiles, which is basically unrelated to 85-GHz T_b.

In summary, the Amazonian precipitation profiles are relatively weak; compared to those in Florida, the convective area fraction, echo-top height, and variability of echoes and vertical motions are all lower. During westerly low-level flow regimes they tend to be weaker and more commonly stratiform than during easterly regimes.

c. Warm rain

The rain-type classification introduced in Part I distinguishes profiles with ''warm'' rain, defined as rain falling from an ice-free cloud. Combined infrared and passive microwave data (Petty 1999) and TRMM PR data (Berg et al. 2002; Schumacher and Houze 2003b) suggest that a significant fraction of the tropical rain results from shallow systems, especially over the oceans peripheral of the intertropical convergence zone, although it is not known how significant warm rain really is. Johnson et al. (1999) suggest that aside from deep convection and shallow cumuli, a third mode of convection prevails in the Tropics, namely, cumulus congestus, with tops at about 5 km. Petty (1999) indicates that 20%–40% of the surface rain reports coincide with minimum satellite infrared temperatures of 273 K or warmer in much of the Tropics. Using wind profiler reflectivity profiles and coincident rain gauge data, Tokay et al. (1999) find that 7% of the rainfall on an atoll in the equatorial west Pacific region results from warm clouds. The detection of warm rain based on TRMM reflectivity profiles is conservative—the TRMM 2A23 algorithm considers warm rain to be certain when the top of the minimum detectable echo is at least 2000 m below the climatological freezing level (NASDA 1999). This definition, which will miss many true warm rain events, is motivated in part by the poor sensitivity of the PR, about 18 dBZ, which implies that the radar cannot see the cloud tops.

A warm rain profile has a 0-dBZ echo top below the freezing level Fig. 2 in Part I). The freezing level is deduced from a proximity sounding. In addition to the operational sondes, many extra sondes were released during all three campaigns. An additional condition for warm rain is that if an anvil is present aloft, then it needs to be separated from the shallow echo by a layer at least 2 km deep with reflectivities less than 0 dBZ. This condition intends to exclude cases where the collision–coalescence process is jump started by the introduction of large droplets from aloft. Such a situation occurs on the northern (right) eyewall in the transect across Hurricane Bonnie (shown in Fig.1)—shallow rain cells are covered by a large anvil, which generally remains clearly separated from the cells. Clearly, a satellite IR-based rainfall estimation technique could not reveal the warm rain under the anvil, but it may be revealed from signature of microwave temperatures, especially the increase in 10-GHz T_b over the warm rain region.

The TRMM PR classifies most isolated, shallow echoes as stratiform; however, because they mostly result from warm cumuli, most of them probably should be classified as convective (Schumacher and Houze

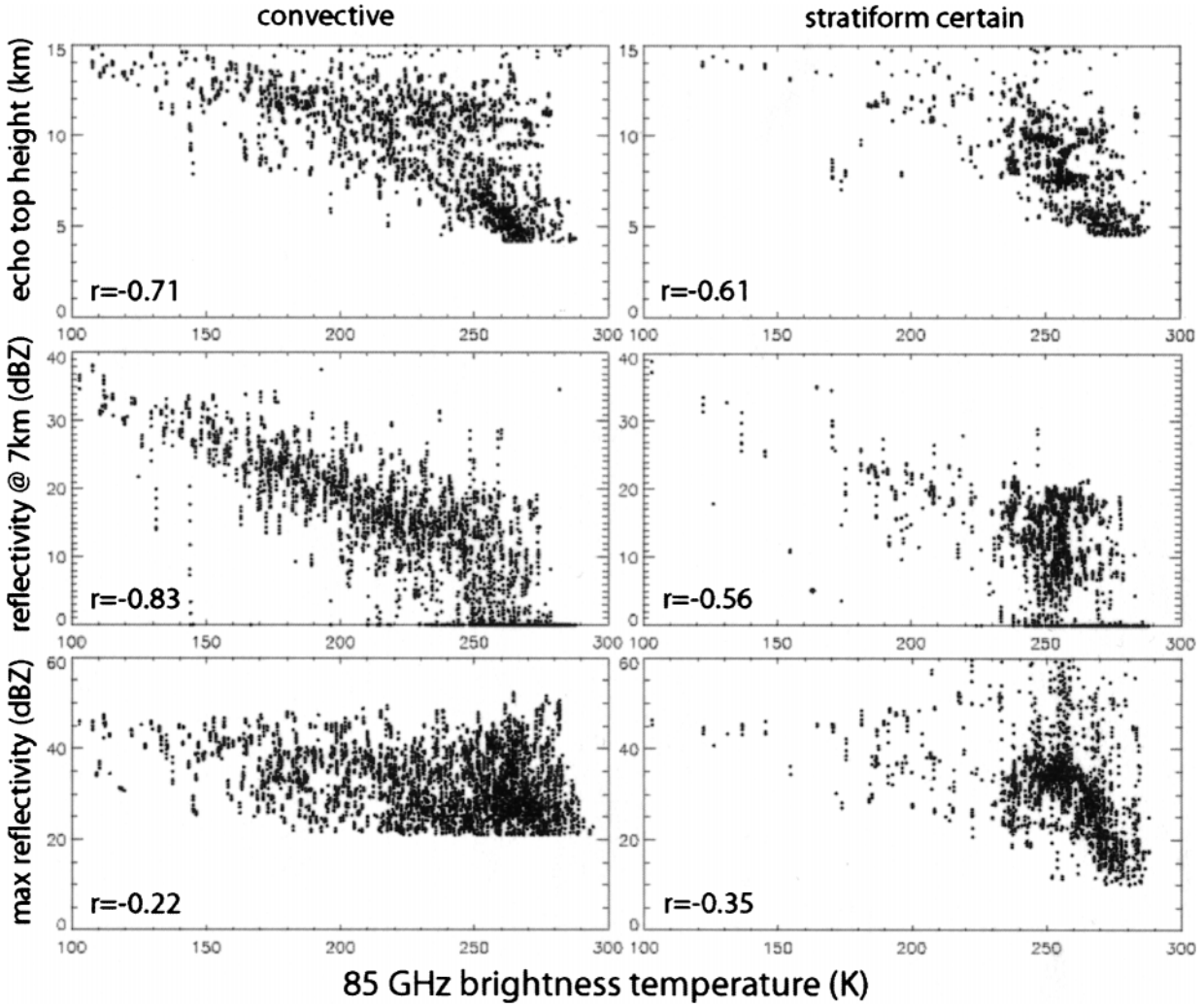

FIG. 11. As Fig. 4, but for all surface rain profiles over Rondonia, Brazil.

2003b). Our classification only defines deep stratiform rain, that is, it contains a BB. By definition warm rain can only be convective or inconclusive. The definition of stratiform precipitation excludes shallow rain systems that are not convective (i.e., driven by buoyancy). Nonconvective warm rain may be rather common in some tropical regions (i.e., where marine stratus is lifted over terrain), but this was not sampled by the ER-2 in any of the three regions.

An example of a flight leg over a series of warm rain cells is shown in Fig. 12. Note that not all of these convective cells are counted as warm rain. The cell near $x = 10$ km, for instance, extends well above the freezing level, and the 85-GHz T_b depression suggests that ice is present in the upper parts of this cell. The cell near $x = 33$ km, however, is classified as warm rain, even though some light snow appears to fall from upper-level clouds. This upper-level echo is at least 2 km above the warm rain cell. Visually, these cells probably appear as cumuli congesti.

Shallow precipitating systems were not targeted in the three ER-2 campaigns used in this study. Nevertheless they were traversed rather frequently, mostly in hurricanes and in Brazil, but rarely in Florida (Table 1). The fraction of surface rain profiles that are warm rain, 4%–8% in the three regions studies, matches the 6%–7% warm rain fraction observed over the western equatorial Pacific [Table 2 in Williams et al. (1992), and Table 2 in Tokay et al. (1999)]. The latter two references refer to the fraction of rain from shallow systems relative to the total rainfall, whereas the percentages in our Table 1 merely refer to a number of occurrences; however, the average rain rate from these shallow systems (3.4 mm h^{-1}) is not much less than the mean rain rate from all storms (4.2 mm h^{-1}; Tokay et al. 1999), so the comparison is valid. ?12

The EDOP warm rain profiles are summarized by means of FADs of nadir beam reflectivity, radial velocity, and derived vertical air motion (Fig. 13). While a broad range of hydrometeor and air vertical motions

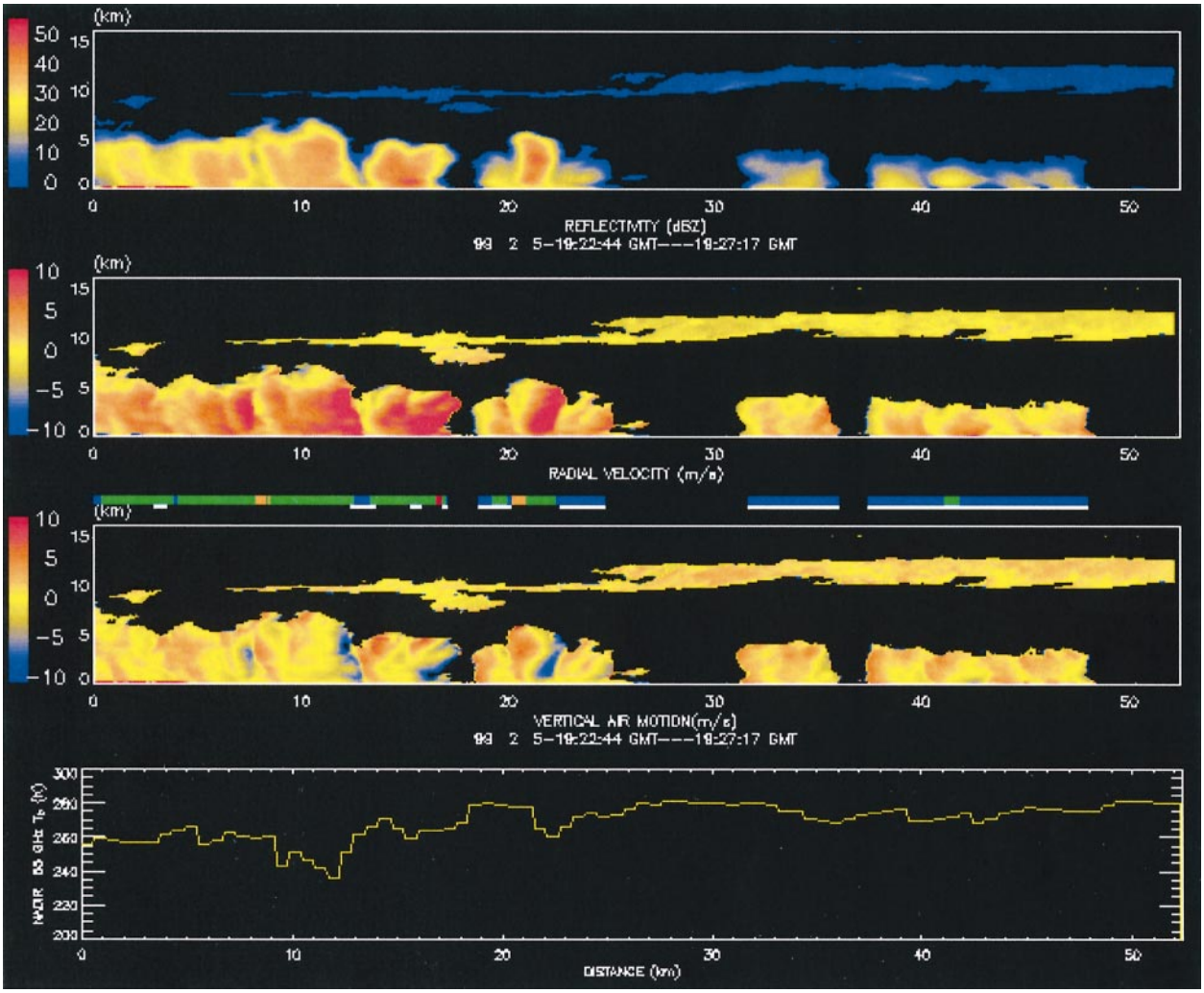

FIG. 12. As Fig. 1, but for a section containing warm rain in Brazil at 1923–1927 UTC 5 Feb 1999. The bottom panel shows the AMPR 85-GHz T_b.

exists in warm rain, the median vertical air motion is slightly positive at all levels, averaging 0.9 m s^{-1}, unlike that in stratiform profiles in Florida and Brazil (Figs. 7 and 9). Comparing the warm rain FAD (Fig. 13) to the FAD for all convective profiles (Fig. 9), both in Brazil, it is clear that the air rises more in the former, compared to the latter. This is consistent with the observation that the reflectivity in warm rain profiles generally increases toward the ground down to about 500 m above ground level (Fig. 13). The downward increase of reflectivity in warm rain, from near the cloud top to low levels, has been observed elsewhere (Williams et al. 1992; Tokay et al. 1999) and contrasts with the profiles of deep precipitation systems, for which reflectivity is rather constant below the freezing level (Figs. 7 and 9). Also, in contrast with deep precipitation systems the reflectivity is generally low, even at low levels; the average value for the Brazil profiles (Fig. 13) at 500 m above ground is only 16.5 dBZ, implying that the TRMM PR, with a sensitivity threshold of 18 dBZ, would fail to capture the majority of these warm rain events. Because most warm rain echoes are rather weak, about half of them are classified as inconclusive (Table 1), based on the profile maximum reflectivity value (Part I). This distinction is arbitrary, and even the weaker warm rain echoes generally appear convective in horizontal structure (Fig. 12).

?13

The prevailing increase in reflectivity and in radial velocity toward the ground, in the case of warm rain (Fig. 13), suggests that raindrops rapidly grow from top to base in shallow systems, which implies an active collision–coalescence process.

4. Discussion

Studies based mainly on TRMM data suggest that significant differences exist in the typical characteristics of convection-generated systems in Florida and Brazil.

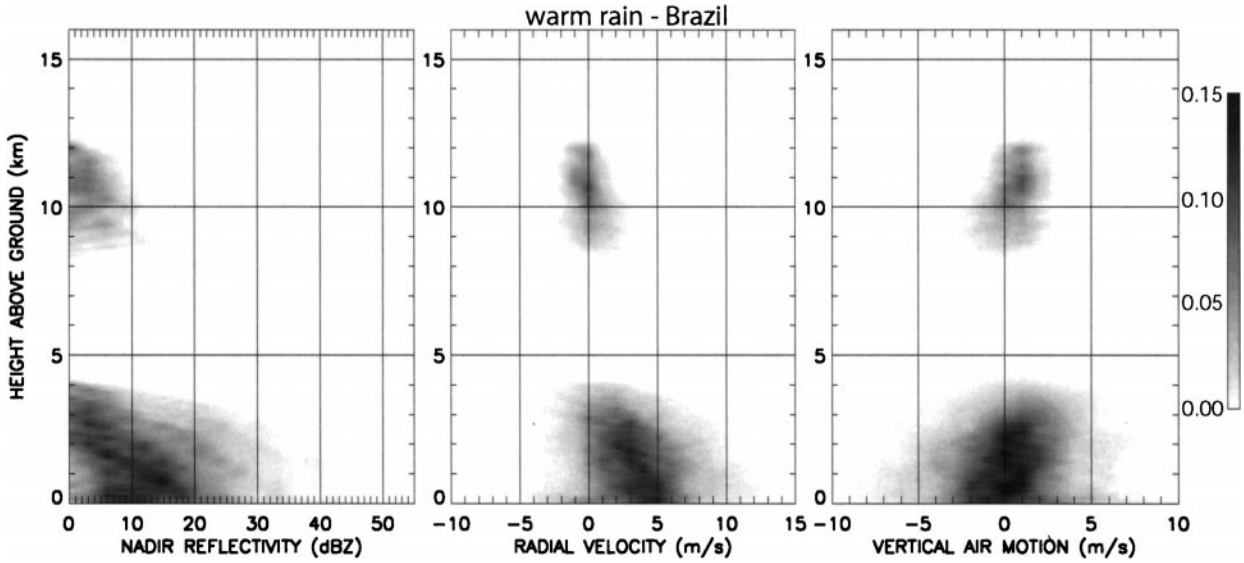

FIG. 13. As Fig. 2, but for all warm rain profiles over Rondonia, Brazil.

These systems tend to be more vigorous over Florida than over the Amazon basin (Petersen and Rutledge 2001). Hurricanes tend to have rather low peak reflectivities and large stratiform regions (Marks 1985; Marks and Houze 1987; Houze et al. 1992).

The airborne dataset used here is small compared to TRMM-based climatologies—too small and selective to attribute much value to the details of the probability density functions of tropical precipitation characteristics. However, Table 2 in Part I confirms that the convective area fraction in Brazil is slightly lower than that in Florida. And the peak reflectivities, the echo tops, and the 7-km reflectivities are highest in Florida (Figs. 2 and 7). Convection is more remarkable in Brazil than in Florida, and the high reflectivities aloft in some of the Florida convection are a testimony of vigorous updrafts.

On the other hand, hurricanes tend to be largely stratiform (Part I). In stratiform regions in hurricanes, compared to those in convection-generated storms in Florida and Brazil, (a) reflectivity decays more rapidly with height above the BB; (b) raindrops continue to grow as they descend; and (c) the mean reflectivity is lower at all levels, at least in comparison with the Florida sample. These three observations confirm a significant difference in stratiform precipitation characteristics observed previously—the convection-generated stratiform regions carry the imprint of strong but transient updrafts, which lift large amounts of ice to upper levels, while those in hurricanes are more uniformly and clearly stratiform, which is consistent with the balanced nature of the hurricane circulation.

These relationships confirm that the relatively small sample used here is representative. This study further complements the TRMM-based climatologies, through the combination of vertical velocity information and passive microwave signatures with high-resolution reflectivity profiles, stratified by rain types. We now further analyze our findings in the context of published findings.

Hurricanes tend to have a higher 85-GHz brightness temperature than convective systems over land (Cecil and Zipser 1999, 2002; Cecil et al. 2002). Mohr and Zipser (1996) find that 69% of the MCSs over tropical South America have a minimum 85-GHz T_b of 200 K or less while that fraction is 66% over North America (a region including but much larger than Florida). These estimates are based on data from the Special Sensor Microwave Imager (SSM/I), whose resolution is about 15 km. Over hurricanes a minimum 85-GHz T_b of 200 K or less is rare (Cecil and Zipser 2002).

Only 4.7% of the hurricane surface rain profiles in this study have a 85-GHz T_b of 200 K or less, compared to 12% for Brazil and 26% for Florida. Stratiform surface rain profiles tend to have a higher 85-GHz T_b compared to convection. Only 3.6% (7.8%) of the hurricane certainly stratiform (convective) surface rain profiles have a 85-GHz T_b of 200 K or less. For Brazil, these percentages are 8.3% (14%), and for Florida 6.0% (35%) for certainly stratiform (convective) profiles. A lower-85-GHz T_b implies a higher ice content. The rather low fraction of convective profiles with 85-GHz T_b of 200 K or less in Brazil is consistent with the relatively weak convection encountered there (section 3b).

TRMM observations indicate that convection-generated systems in the Amazon basin have more ''maritime'' characteristics, while those over Florida are clearly continental (Nesbitt et al. 2000; Petersen and Rutledge 2001; Toracinta et al. 2002). The maritime character of convection-generated storms can be expressed most clearly in terms of their lightning activity, which is low over the oceans (Orville and Hendersen

1986; Goodman and Christian 1993; Petersen and Rutledge 2001). Moreover, an oceanic storm with the same apparent intensity as a continental storm is less likely to produce lightning (Toracinta et al. 2002). Here the intensity is measured either in terms of the maximum height of a radar reflectivity threshold, or in terms of the minimum 85-GHz T_b. Lightning over the ocean is believed to be rare because the updrafts are too weak to loft sufficient amounts of graupel into the mixed-phase region of the cloud (Williams et al. 1992). In situ aircraft observations have shown that strong updrafts are indeed rare in convection-generated storms over the ocean (Zipser and LeMone 1980; Lucas et al. 1994). The strongest updrafts in oceanic storms are less than half as strong as the same top percentile of updrafts in storms over land (Jorgensen and LeMone 1989).

The EDOP dataset does confirm that strong updrafts are more common over Florida than over Rondonia. An updraft of at least 4 m s^{-1} can be considered to be a threshold for lightning. In Florida 6% of the convective profiles have updrafts strong enough to loft hydrometeors at 4 m s^{-1} or more, and all of these are above the freezing level (Fig. 7, Table 4 in Part I). That figure is 3% in Brazil (Fig. 9). Two cautionary remarks are warranted here. First, these percentages are affected by a $\sim$2 m s^{-1} error bracket due to uncertainties in the correction for aircraft motion and the estimation of terminal velocity V_t (Part I). And second, the differences in extreme updraft frequency in the two regions may be affected by differences in Z–V_t relationships. In short, the EDOP/AMPR observations in Brazil and Florida are broadly consistent with recent satellite-based studies of tropical precipitation systems, and the EDOP Doppler velocity profiles confirm that strong updrafts are most common in central Florida.

5. Summary

Measurements of vertical incidence radar reflectivity and radial velocity, as well as coincident upwelling microwave radiances, are analyzed for 21 231 km of flight tracks of the high-altitude ER-2 aircraft over tropical precipitation systems. The systems sampled were preferentially deep, long-lived, large, and occurred in the afternoon. Shallow precipitation systems were encountered even though they were not targeted. The tendency for warm rain reflectivity and radial velocity to increase toward the ground suggests that raindrops rapidly grow from top to base in shallow systems.

The classification introduced in Part I is used to contrast convective hydrometeor profiles against stratiform ones. The data are divided in tropical cyclones or depressions over the Atlantic (''hurricane''), and convection-generated storms in central Florida (''Florida'') and in the state of Rondonia in the southwestern Amazon basin (''Brazil''). While the sample is too small and selective to represent a climatology of tropical precipitation systems, the dataset is complementary to TRMM measurements mainly because of EDOP's superior vertical resolution and sensitivity, and because EDOP yields vertical velocity estimates. The EDOP-based profiles of reflectivity, hydrometeor settling speeds, and vertical air motion, and their relationship with the coincident AMPR 85-GHz brightness temperature (T_b), yield insights that confirm and extend TRMM-based characterizations of precipitation systems in these regions. Key conclusions are as follows:

- Rain-type regions in hurricanes are significantly different from those in convection-generated storms. Hurricanes are largely stratiform—their reflectivity and vertical velocity profiles are quite uniform. Their reflectivity decays rapidly with height above the bright band, and below the bright band it increases slightly toward the ocean surface. Convective regions in hurricanes are not fundamentally different from stratiform regions; the reflectivity and vertical velocity variability is rather small and the reflectivity profile shows a clear kink at the melting level. Hurricanes have a relatively high 85-GHz T_b, a relatively high fraction of warm rain profiles, and generally experience ascending air motion at all levels, even in stratiform regions.
- Convective regions are about as common as stratiform regions in Florida storms. Convection can be vigorous, yielding high reflectivity values aloft, and very low 85-GHz T_b values. Florida stratiform regions are relatively small and highly variable in terms of vertical velocity and echo strength. This suggests that they carry the imprint of the convection that generated them, and that they are short lived. They tend to experience ascent above the BB and subsidence below. They are characterized by higher reflectivities at upper levels and a lower 85-GHz T_b, compared to stratiform regions in Brazil. The Brazil sample is more maritime than the Florida sample, in terms of convective area fraction, echo-top height, and variability of echoes and vertical motions. The storms sampled during westerly low-level wind regimes in Brazil were generally weaker and the stratiform area fraction was larger.
- Finally, we found that in both hurricanes and convection-generated storms a higher reflectivity at 7 km and a higher echo top, well above the freezing level, generally imply a lower 85-GHz T_b. These correlations are stronger for convective than for stratiform regions. The 85-GHz T_b correlates more poorly with the profile maximum reflectivity.

Acknowledgments. This work was supported by NASA EPSCoR Grant 5-33395. We appreciate the data-processing support of Q. Miao, the assistance of Dr. G. Heymsfield, and the review comments of Dr. R. A. Houze.

REFERENCES

Berg, W., C. Kummerow, and C. A. Morales, 2002: Differences between east and west Pacific rainfall systems. *J. Climate,* **15,** 3659–3672.

Bister, M., and K. A. Emanuel, 1997: The genesis of Hurricane Guillermo: TEXMEX analyses and a modeling study. *Mon. Wea. Rev.,* **125,** 2662–2682.

Cecil, D. J., and E. J. Zipser, 1999: Relationships between tropical cyclone intensity and satellite-based indicators of inner core convection: 85-GHz ice-scattering signature and lightning. *Mon. Wea. Rev.,* **127,** 103–123.

——, and ——, 2002: Reflectivity, ice scattering, and lightning characteristics of hurricane eyewalls and rainbands. Part II: Intercomparison of observations. *Mon. Wea. Rev.,* **130,** 785–801.

——, ——, and S. W. Nesbitt, 2002: Reflectivity, ice scattering, and lightning characteristics of hurricane eyewalls and rainbands. Part I: Quantitative description. *Mon. Wea. Rev.,* **130,** 769–784.

Cheng, C., and R. A. Houze Jr., 1979: The distribution of convective and mesoscale precipitation in GATE radar echo patterns. *Mon. Wea. Rev.,* **107,** 1370–1381.

Chong, M., and J. Testud, 1983: Three-dimensional wind field analysis from dual-Doppler radar data. Part III: The boundary condition: An optimum determination based on a variational concept. *J. Climate Appl. Meteor.,* **22,** 1227–1241.

——, and D. Hauser, 1989: A tropical squall line observed during the COPT 81 experiment in West Africa. Part II: Water budget. *Mon. Wea. Rev.,* **117,** 728–744.

Churchill, D. D., and R. A. Houze Jr., 1984: Development and structure of winter monsoon cloud clusters on 10 December 1978. *J. Atmos. Sci.,* **41,** 933–960.

Geerts, B., and Y. Dawei, 2004: Classification and characterization of tropical precipitation based on high-resolution airborne vertical incidence radar. Part I: Classification. *J. Appl. Meteor.,* in press.

——, G. M. Heymsfield, L. Tian, J. B. Halverson, A. Guillory, and M. I. Mejia, 2000: Hurricane Georges' landfall in the Dominican Republic: Detailed airborne Doppler radar imagery. *Bull. Amer. Meteor. Soc.,* **81,** 999–1018.

Goldenberg, S. B., R. A. Houze Jr., and D. D. Churchill, 1990: Convective and stratiform components of a winter monsoon cloud cluster determined from geosynchronous IR satellite data. *J. Meteor. Soc. Japan.,* **68,** 37–63.

Goodman, S. J., and H. Christian, 1993: Global observations of lightning. *Atlas of Satellite Observations Related to Global Change,* R. J. Gurney, J. L. Foster, and C. L. Parkinson, Cambridge University Press, 191–219.

Halverson, J. B., T. Rickenbach, B. Roy, H. Pierce, and E. Williams, 2002: Environmental characteristics of convective systems during TRMM-LBA. *Mon. Wea. Rev.,* **130,** 1493–1509.

Heymsfield, G. M., and Coauthors, 1996: The EDOP radar system on the high-altitude NASA ER-2 aircraft. *J. Atmos. Oceanic Technol.,* **13,** 795–809.

Houze, R. A., Jr., 1993: *Cloud Dynamics.* Academic Press, 573 pp.

——, 1997: Stratiform precipitation in regions of convection: A meteorological paradox? *Bull. Amer. Meteor. Soc.,* **78,** 2179–2196.

——, F. D. Marks, and R. A. Black, 1992: Dual-aircraft investigation of the inner core of Hurricane Norbert. Part II: Mesoscale distribution of ice particles. *J. Atmos. Sci.,* **49,** 943–963.

Johnson, R. H., T. M. Rickenbach, S. A. Rutledge, P. E. Ciesielski, and W. H. Schubert, 1999: Trimodal characteristics of tropical convection. *J. Climate,* **12,** 2397–2418.

Jorgensen, D. P., 1984: Mesoscale and convective-scale characteristics of mature hurricanes. Part I: General observations by research aircraft. *J. Atmos. Sci.,* **41,** 1268–1286.

——, and M. A. LeMone, 1989: Vertically velocity characteristics of oceanic convection. *J. Atmos. Sci.,* **46,** 621–640.

Kingsmill, D. E., 1995: Convection initiation associated with a seabreeze front, a gust front, and their collision. *Mon. Wea. Rev.,* **123,** 2913–2933.

Kummerow, C., I. M. Hakkarinen, H. F. Pierce, and J. A. Weinman, 1991: Determination of precipitation profiles from airborne passive microwave radiometric measurements. *J. Atmos. Oceanic Technol.,* **8,** 148–158.

——, and Coauthors, 2000: The status of the Tropical Rainfall Measuring Mission (TRMM) after two years in orbit. *J. Appl. Meteor.,* **39,** 1965–1982.

Leary, C. A., 1984: Precipitation structure of the cloud clusters in a tropical easterly wave. *Mon. Wea. Rev.,* **112,** 313–325.

Lucas, C., E. J. Zipser, and M. A. LeMone, 1994: Vertical velocity in oceanic convection off tropical Australia. *J. Atmos. Sci.,* **51,** 3183–3193.

Marks, F. D., 1985: Evolution of the structure of precipitation in Hurricane Allen (1980). *Mon. Wea. Rev.,* **113,** 909–930.

——, and R. A. Houze Jr., 1987: Inner core structure of Hurricane Alicia from airborne Doppler radar observations. *J. Atmos. Sci.,* **44,** 1296–1317.

Mohr, K. I., and E. J. Zipser, 1996: Defining mesoscale convective systems by their 85-GHz ice-scattering signatures. *Bull. Amer. Meteor. Soc.,* **77,** 1179–1190.

——, J. S. Famiglietti, and E. J. Zipser, 1999: The contribution to tropical rainfall with respect to convective system type, size, and intensity estimated from the 85-GHz ice-scattering signature. *J. Appl. Meteor.,* **38,** 596–606.

NASDA, 1999: TRMM PR algorithm instruction manual V1.0. Communications Research Laboratory, 52 pp. [Available from Communications Research Laboratory, 4-2-1 Nukui-kitamachi, Koganei-chi, Tokyo 184, Japan.]

Nesbitt, S. W., and E. J. Zipser, 2003: The diurnal cycle of rainfall and convective intensity according to three years of TRMM measurements. *J. Climate,* **16,** 1456–1475. ?14

——, ——, and D. J. Cecil, 2000: A census of precipitation features in the Tropics using TRMM: Radar, ice scattering, and lightning observations. *J. Climate,* **13,** 4087–4106.

Orville, R. E., and R. W. Henderson, 1986: Global distribution of midnight lightning: September 1977 to August 1978. *Mon. Wea. Rev.,* **114,** 2640–2653.

Petersen, W. A., and S. A. Rutledge, 2001: Regional variability in tropical convection: Observations from TRMM. *J. Climate,* **14,** 3566–3586.

——, S. W. Nesbitt, R. J. Blakeslee, R. Cifelli, P. Hein, and S. A. Rutledge, 2002: TRMM observations of intraseasonal variability in convective regimes over the Amazon. *J. Climate,* **15,** 1278–1294.

Petty, G. W., 1999: Prevalence of precipitation from warm-topped clouds over eastern Asia and the western Pacific. *J. Climate,* **12,** 220–229.

Rickenbach, T. M., and S. A. Rutledge, 1998: Convection in TOGA COARE: Horizontal scale, morphology, and rainfall production. *J. Atmos. Sci.,* **55,** 2715–2729.

——, R. N. Ferreira, J. B. Halverson, D. L. Herdies, and M. A. F. Silva Dias, 2002: Modulation of convection in the southwestern Amazon basin by extratropical stationary fronts. *J. Geophys. Res.,* **107,** 8040, doi:10.1029/2000JD000263.

Schumacher, C., and R. A. Houze Jr., 2003a: Stratiform rain in the Tropics as seen by the TRMM Precipitation Radar. *J. Climate,* **16,** 1739–1756.

——, and ——, 2003b: The TRMM precipitation radar's view of shallow, isolated rain. *J. Appl. Meteor.,* **42,** 1519–1524.

Short, D. A., P. A. Kucera, B. S. Ferrier, J. C. Gerlach, S. A. Rutledge, and O. W. Thiele, 1997: Shipboard radar rainfall patterns within the TOGA COARE IFA. *Bull. Amer. Meteor. Soc.,* **78,** 2817–2836.

Spencer, R. W., R. E. Hood, F. J. LaFontaine, E. A. Smith, R. Platt, J. Galliano, V. L. Griffin, and E. Lobl, 1994: High-resolution imaging of rain systems with the Advanced Microwave Precipitation Radiometer. *J. Atmos. Oceanic Technol.,* **11,** 849–857.

Steiner, M., R. A. Houze, and S. E. Yuter, 1995: Climatological characterization of three-dimensional storm structure from operational radar and rainguage data. *J. Appl. Meteor.,* **34,** 1978–2007.

Stewart, R. E., J. D. Marwitz, J. C. Pace, and R. E. Carbone, 1984: Characteristics through the melting layer of stratiform clouds. ?15 *J. Atmos. Sci.,* **41,** 3227–3237.

Tokay, A., D. A. Short, C. R. Williams, W. L. Ecklund, and K. L. Gage, 1999: Tropical rainfall associated with convective and stratiform clouds: Intercomparison of disdrometer and profiler measurements. *J. Appl. Meteor.,* **38,** 302–320.

Toracinta, E. R., D. J. Cecil, E. J. Zipser, and S. W. Nesbitt, 2002: Radar, passive microwave, and lightning characteristics of precipitating systems in the Tropics. *Mon. Wea. Rev.,* **130,** 802–824.

Williams, E. R., S. A. Rutledge, S. G. Geotis, N. Renno, E. Rasmussen, and T. Rickenbach, 1992: A radar and electrical study of tropical ''hot towers.'' *J. Atmos. Sci.,* **49,** 1386–1396.

Willoughby, H. E., F. D. Marks, and R. J. Feinberg, 1984: Stationary and moving convective bands in hurricanes. *J. Atmos. Sci.,* **41,** 3189–3211.

Yuter, S. E., and R. A. Houze, 1998: The natural variability of precipitating clouds over the western Pacific warm pool. *Quart. J. Roy. Meteor. Soc.,* **124,** 53–99.

——, and ——, 2003: Microphysical modes of precipitation growth determined by S-band vertically pointing radar in orographic precipitation during MAP. *Quart. J. Roy. Meteor. Soc.,* **129,** 455–476. ?16

Zipser, E. J., and M. A. LeMone, 1980: Cumulonimbus vertical velocity events in GATE. Part II: Synthesis and model core structure. *J. Atmos. Sci.,* **37,** 2458–2469.